



Article

Brillouin Klein space and half-turn space in three-dimensional acoustic crystals

Zhenxiao Zhu ^{a,1}, Linyun Yang ^{a,1}, Jien Wu ^{b,1}, Yan Meng ^a, Xiang Xi ^a, Bei Yan ^a, Jingming Chen ^a, Jiuyang Lu ^{b,c}, Xueqin Huang ^b, Wei Yin Deng ^{b,c}, Ce Shang ^d, Perry Ping Shum ^a, Yihao Yang ^e, Hongsheng Chen ^e, Kexin Xiang ^a, Gui-Geng Liu ^{f,*}, Zhengyou Liu ^{c,g,*}, Zhen Gao ^{a,*}

^a State Key Laboratory of Optical Fiber and Cable Manufacture Technology, Department of Electronic and Electrical Engineering, Southern University of Science and Technology, Shenzhen 518055, China

^b School of Physics and Optoelectronics, South China University of Technology, Guangzhou 510640, China

^c Key Laboratory of Artificial Micro- and Nanostructures of Ministry of Education and School of Physics and Technology, Wuhan University, Wuhan 430072, China

^d King Abdullah University of Science and Technology (KAUST), Physical Science and Engineering Division (PSE), Thuwal 23955-6900, Saudi Arabia

^e Interdisciplinary Center for Quantum Information, State Key Laboratory of Modern Optical Instrumentation, ZJU-Hangzhou Global Science and Technology Innovation Center, College of Information Science and Electronic Engineering, ZJU-UIUC Institute, Zhejiang University, Hangzhou 310027, China

^f Division of Physics and Applied Physics, School of Physical and Mathematical Sciences, Nanyang Technological University, Singapore 637371, Singapore

^g Institute for Advanced Studies, Wuhan University, Wuhan 430072, China

ARTICLE INFO

Article history:

Received 1 February 2024

Received in revised form 28 March 2024

Accepted 6 May 2024

Available online 11 May 2024

Keywords:

Momentum-space non-symmorphic

symmetry

Brillouin Klein space and half-turn space

Acoustic Klein bottle insulator

Self-collimated topological surface states

ABSTRACT

The Bloch band theory and Brillouin zone (BZ) that characterize wave-like behaviors in periodic mediums are two cornerstones of contemporary physics, ranging from condensed matter to topological physics. Recent theoretical breakthrough revealed that, under the projective symmetry algebra enforced by artificial gauge fields, the usual two-dimensional (2D) BZ (orientable Brillouin two-torus) can be fundamentally modified to a non-orientable Brillouin Klein bottle with radically distinct manifold topology. However, the physical consequence of artificial gauge fields on the more general three-dimensional (3D) BZ (orientable Brillouin three-torus) was so far missing. Here, we theoretically discovered and experimentally observed that the fundamental domain and topology of the usual 3D BZ can be reduced to a non-orientable Brillouin Klein space or an orientable Brillouin half-turn space in a 3D acoustic crystal with artificial gauge fields. We experimentally identify peculiar 3D momentum-space non-symmorphic screw rotation and glide reflection symmetries in the measured band structures. Moreover, we experimentally demonstrate a novel stacked weak Klein bottle insulator featuring a nonzero \mathbb{Z}_2 topological invariant and self-collimated topological surface states at two opposite surfaces related by a nonlocal twist, radically distinct from all previous 3D topological insulators. Our discovery not only fundamentally modifies the fundamental domain and topology of 3D BZ, but also opens the door towards a wealth of previously overlooked momentum-space multidimensional manifold topologies and novel gauge-symmetry-enriched topological physics and robust acoustic wave manipulations beyond the existing paradigms.

© 2024 Science China Press. Published by Elsevier B.V. and Science China Press. All rights are reserved, including those for text and data mining, AI training, and similar technologies.

1. Introduction

Since their introduction in 1929, the Bloch band theory [1] and Brillouin zone (BZ) [2] that characterize wave-like behaviors in periodic mediums have played a central role in condensed matter

physics [3,4] and artificial crystals such as metamaterials [5,6], photonic crystals [7–15], acoustic crystals [16–30], electric circuits [31,32], mechanical networks [33–35], and cold-atom lattices [36]. Particularly, they are essential in the discovery and classification of topological phases of matter whose band topologies and topological invariants are usually defined on a two-dimensional (2D) BZ (Brillouin two-torus) [10–13,18–25] or a three-dimensional (3D) BZ (Brillouin three-torus) [14,15,26–28]. For example, the celebrated topological invariant characterizing the Chern insulators (Chern number) is defined by integrating the Berry curvatures over

* Corresponding authors.

E-mail addresses: guigeng001@e.ntu.edu.sg (G.-G. Liu), zyliu@whu.edu.cn (Z. Liu), gaoz@sustech.edu.cn (Z. Gao).

¹ These authors contributed equally to this work.

the Brillouin two-torus surface [12,15,35,36]. Consequently, the multidimensional manifold topology of the BZ itself is crucial for the exploration of topological physics. So far, the topological phases of matter are mainly classified and characterized over the orientable Brillouin two (three)-torus.

Meanwhile, gauge symmetry that projectively represents the algebraic structure of crystalline symmetries has fundamentally modified topological physics and greatly enriched the topological phases of matter [37–47], such as Möbius-twisted topological phases with projective translation symmetry [38–40], spinless mirror Chern insulators with projective mirror symmetry [41,42], topological phases switching [43,44] and high-order Stiefel-Whitney semimetals [46,47] with projective spacetime inversion (PT) symmetry. Although the symmetries of those systems were projectively represented beyond the group theory for crystal symmetries, the fundamental domain and topology of BZ (orientable Brillouin two-torus or three-torus) based on which to define the topological invariants and classify the topological states remain unchanged. Remarkably, recent theoretical work [48] unveiled that the fundamental domain and topology of 2D momentum space can be modified by artificial gauge fields from a usual orientable Brillouin two-torus to a non-orientable Brillouin Klein bottle, resulting in novel 2D Klein bottle insulators. A space manifold is non-orientable if it contains a close path that brings a traveler back to his starting point mirror-reversed (such as Klein bottle, Möbius strip), otherwise, it is orientable (such as spheres, torus). Since the manifold topology of the BZ itself is crucial for exploring topological physics, it is natural to ask what is the physical consequence of artificial gauge fields on the more general 3D BZ. Will it generate any new momentum-space three-manifold topology that has never been witnessed in conventional 3D periodic physical systems?

Here, we theoretically discovered and experimentally observed that the fundamental domain and topology of the 3D BZ can be reduced from an orientable Brillouin three-torus to a non-orientable Brillouin Klein space or an orientable half-turn space [49] in a 3D acoustic crystal with artificial gauge fields. Moreover, we directly observe non-symmorphic screw rotation and glide reflection symmetries in 3D momentum space, giving rise to a novel stacked weak Klein bottle insulator with a non-zero \mathbb{Z}_2 topological invariant and two self-collimated topological surface states related by a nonlocal twist. Interestingly, we experimentally demonstrate that the previously discovered Brillouin Klein bottle [48] can be observed in Brillouin Klein space or half-turn space in 3D momentum space when appropriately cut.

2. Methods

2.1. Simulations

All numerical simulations of the 3D acoustic crystal are performed using the acoustic module of COMSOL Multiphysics. The background medium (air) is modeled with a density of 1.18 kg m^{-3} and a sound speed of 346 m s^{-1} . The plastic stereolithography can be considered as hard boundaries due to substantial acoustic impedance contrast compared with air. Bulk band structures are calculated by using a unit cell with periodic boundary conditions along all three directions. Surface state dispersions are calculated by using a supercell that consists of 15 unit cells with periodic boundary conditions along the y and z directions and hard boundary conditions along the x direction.

2.2. Experimental measurements

The experimental sample was fabricated by 3D printing with photopolymer materials which consists of $15 \times 15 \times 15$ unit cells.

The materials are photosensitive resin with a modulus of 2880 MPa and a density of 1.10 g cm^{-3} . The structure can be viewed as hard walls for the acoustic waves that propagate in the acoustic crystal due to the large impedance mismatch between air and the resin material. A small hole with radius of 2 mm is located at the center of each resonator for excitation and detection. When not in use, they are blocked by plugs. In the experiment, the acoustic signal is launched from a headphone placed at the bulk (surface) of the sample to excite the acoustic bulk (surface) modes. A microphone attached to the tip of a stainless-steel rod is inserted into each resonator to measure the acoustic signals one by one. Both the source and probe are connected to a vector network analyzer (Keysight E5061B) for the generation and recording of the sound signals. Spatial Fourier transforms are applied to the measured complex acoustic field distributions to obtain the measured *iso*-frequency contours and dispersion relations.

3. Results and discussion

3.1. Momentum-space screw rotation and glide reflection symmetries

We first construct a cubic lattice model with a unit cell consisting of four sites (beige spheres) coupled with positive (dark green cylinders) and negative (red cylinders) intralayer couplings, and the neighboring layers are coupled with positive interlayer chiral couplings (slanted dark green cylinders), as shown in Fig. 1a. The insets present the lattice model's top view (x - y plane) with each plaquette enclosing a π gauge flux and the front view (x - z plane) with chiral interlayer couplings. Under the spatial mirror symmetry M_x (M_z) in the x (z) direction (dashed lines refer to the mirror planes), the distribution of gauge flux is invariant but the intralayer coupling sign and the interlayer coupling configuration are exchanged. Therefore, the projective representation of spatial two-fold rotation symmetries composed of two mirror symmetries M_x and M_z is accompanied by a gauge transformation G , and the rotation symmetry is modified to $\mathbf{R}_y = G\mathbf{R}_y$. While under the translation symmetry L_y (L_z) with period a (h) along the y (z) direction, both the gauge flux and the coupling sign remain unchanged. Consequently, the translation symmetry in the y (z) direction is represented as $\mathbf{L}_y = L_y$ ($\mathbf{L}_z = L_z$) without accompanying G . Note that the gauge sign of each site will be exchanged when the gauge transformation G is translated a (h) in the y (z) direction (the bottom panel of Fig. 1a), respectively. The algebraic relation will be projectively represented as

$$\mathbf{R}_y \mathbf{L}_y \mathbf{R}_y^{-1} = -\mathbf{L}_y, \quad \mathbf{R}_y \mathbf{L}_z \mathbf{R}_y^{-1} = -\mathbf{L}_z^{-1}, \quad (1)$$

where \mathbf{R}_y can be regarded as a momentum-space screw rotation along the k_y direction followed by a translation $(\mathbf{G}_y + \mathbf{G}_z)/2$. Consequently, the eigenenergy at (k_x, k_y, k_z) is equivalent to that at $(-k_x, k_y + \pi, -k_z + \pi)$ for the model (see Supplementary materials for detailed explanations), indicating that only half of the 3D BZ partitioned by a fixed k_y (green plane) is independent which can be regarded as the fundamental domain of the 3D momentum space, as shown in Fig. 1b. The feature of 3D momentum-space non-symmorphic screw rotation symmetry can be clearly observed in the constant energy surfaces and energy contours of the model. In Fig. 1d, the constant energy surfaces in the back half 3D BZ (pink sheets) can be achieved by rotating that in the front half 3D BZ (purple sheets) at 180° around the k_y axis (red line). Fig. 1e, f show the constant energy contours at fixed $k_y = -0.5\pi$ and $k_y = -0.5\pi + \pi$, respectively. The pink (purple) dashed lines in Fig. 1e (Fig. 1f) can be obtained by rotating the purple (pink) solid lines 180° around the k_y axis, which are exactly the pink (purple) solid lines in Fig. 1f (Fig. 1e). Note that this result holds for any k_y and $k_y + \pi$ (see the Supplementary materials). Hence, by “gluing” the front

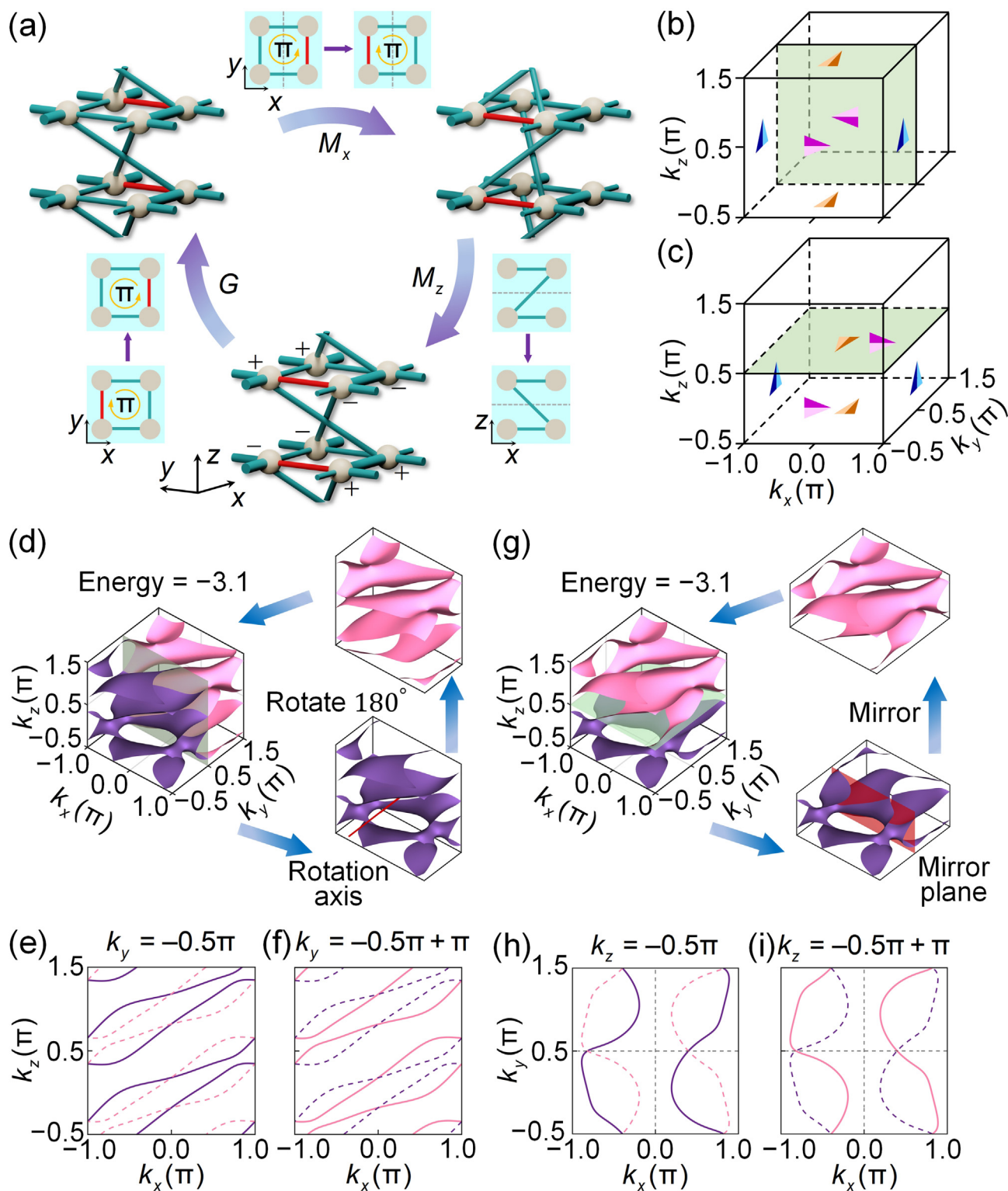


Fig. 1. Brillouin half-turn space and Klein space for a cubic lattice model. (a) The tight-binding configuration is invariant under the spatial mirror operations M_x and M_z in the x and z directions and the gauge transformation G . (b) Brillouin half-turn space with 3D momentum-space screw rotation symmetry. (c) Brillouin Klein space with 3D momentum-space glide reflection symmetry. The direction and the light and dark color of the arrows indicate how the opposite faces of the half 3D BZ will be “glued” together. The momentum-space screw rotation and glide reflection symmetries of the constant energy surfaces of the cubic lattice model are shown in (d) and (g), respectively. (e, f) The constant energy contours with fixed $k_y = -0.5\pi$ and $k_y = -0.5\pi + \pi$, respectively. (h, i) The constant energy contours with fixed $k_z = -0.5\pi$ and $k_z = -0.5\pi + \pi$, respectively.

(k_y) and back faces ($k_y + \pi$) of the half 3D BZ with a 180° rotation around the k_y axis and the other two pairs of opposite faces in the usual way, the half 3D BZ here is topologically an orientable half-turn space.

Note that the eigenenergy at (k_x, k_y, k_z) is equivalent to that at $(k_x, \pi - k_y, k_z + \pi)$ due to the time-reversal symmetry of the whole system (see the [Supplementary materials](#)). This indicates that the 3D BZ can also be partitioned into two parts by a fixed k_z (green

plane) and only half of the 3D BZ is independent as the fundamental domain of the 3D momentum space, as shown in Fig. 1c. 3D momentum-space non-symmorphic glide reflection symmetry can be observed in the constant energy surfaces and energy contours of the model. As shown in Fig. 1g, by mirroring the constant energy surfaces in the lower half 3D BZ (purple sheets) around $k_y = 0.5\pi$ (red plane), we can achieve the constant energy surfaces in the upper half 3D BZ (pink sheets). The constant energy contours at fixed $k_z = -0.5\pi$ and $k_z = -0.5\pi + \pi$ are plotted in Fig. 1h and i, respectively. The pink (purple) dashed lines in Fig. 1h (Fig. 1i) can be obtained by reflecting the purple (pink) solid lines through $k_y = 0.5\pi$ (horizontal grey dashed line), which are exactly the pink (purple) solid lines in Fig. 1i (Fig. 1h). Thus, by “gluing” the bottom (k_z plane) and top ($k_z + \pi$ plane) faces of the half 3D BZ with k_y axis flip and the other two pairs of opposite faces with the usual way, the half 3D BZ here is topologically a non-orientable Klein space (see Supplementary materials). It is worth noting that the glide reflection here is an anti-unitary symmetry, which is different from the case in Ref. [48]. Counterintuitively, we realize both orientable Brillouin half-turn space and non-orientable Klein space in the same model by partitioning the original 3D BZ into two parts along different (k_y or k_z) directions.

Notably, by appropriately cutting the Brillouin half-turn space (Fig. 2a, b) or Klein space (Fig. 2c, d), the obtained fundamental domain of the cut 2D BZ (cyan planes) can be “glued” together with the topology of a non-orientable Klein bottle. In Fig. 2e, f (Fig. 2g, h), the reflection of the constant energy contours in the lower half cut 2D BZ through the k_y (k_z) axis (vertical grey dashed lines) followed by a half translation $\mathbf{L}_{G_y/2}$ ($\mathbf{L}_{G_z/2}$) coincides with the constant energy contours in the upper half cut 2D BZ, demonstrating the 2D momentum-space glide reflection symmetry of the Brillouin Klein bottle. Besides, more Brillouin Klein bottles can be cut from the Brillouin half-turn space if the two oppositely oriented boundaries (magenta lines) of the fundamental domain of the cut 2D BZ (green plane) in Fig. 2a (Fig. 2b) move along opposite k_z (k_x) directions

with the same wave vector or cut from Brillouin Klein space in Fig. 2c, d with any fixed k_x (see the Supplementary materials).

3.2. Observation of Brillouin half-turn space and Klein space in acoustic crystal

We then experimentally demonstrate the Brillouin half-turn space and Klein space in a 3D acoustic crystal. The experimental sample consists of $30 \times 30 \times 15$ acoustic resonators, as shown in Fig. 3a. Each unit cell consists of four cylindrical acoustic resonators (beige color) with a radius of r_0 and heights of h_1 and h_2 , as illustrated in Fig. 3b. Straight tubes with radii of r_1 to r_5 connecting four acoustic resonators serve as the positive (dark green color) or negative (red color) intralayer couplings, and the dark green curved tubes with a radius of r_6 serve as the positive interlayer chiral couplings. Fig. 3d, e present the measured (color maps) and simulated (green lines) iso-frequency contours at 6.46 kHz with fixed $k_y = -0.5\pi/a$ (orange-red plane in Fig. 3c) and $k_y = -0.5\pi/a + \pi/a$ (blue plane in Fig. 3c), respectively. Remarkably, after rotating one of the two iso-frequency contours by 180° around the k_y axis (normal vector of the k_x - k_z plane), it will coincide exactly with the other one. Moreover, this conclusion applies to any fixed k_y ranging from $-0.5\pi/a$ to $0.5\pi/a$ (see Supplementary materials), indicating that the half 3D BZ is topologically an orientable Brillouin half-turn space. Particularly, by cutting the Brillouin half-turn space appropriately, we can obtain non-orientable Brillouin Klein bottles over which the band structure exhibits 2D momentum-space glide reflection symmetry. As shown in Fig. 3f, with fixed $k_x = 0$ (yellow plane in Fig. 3c), the reflection of the measured iso-frequency contour over the cut lower half 2D BZ $k_z \in [-0.5\pi/h, 1.5\pi/h] \times k_y \in [-0.5\pi/a, 0.5\pi/a]$ through the $k_z = 0.5\pi/h$ axis (vertical grey dashed line) coincides with that over the cut upper half 2D BZ $k_z \in [-0.5\pi/h, 1.5\pi/h] \times k_y \in [0.5\pi/a, 1.5\pi/a]$ after a half translation $\mathbf{L}_{G_y/2}$.

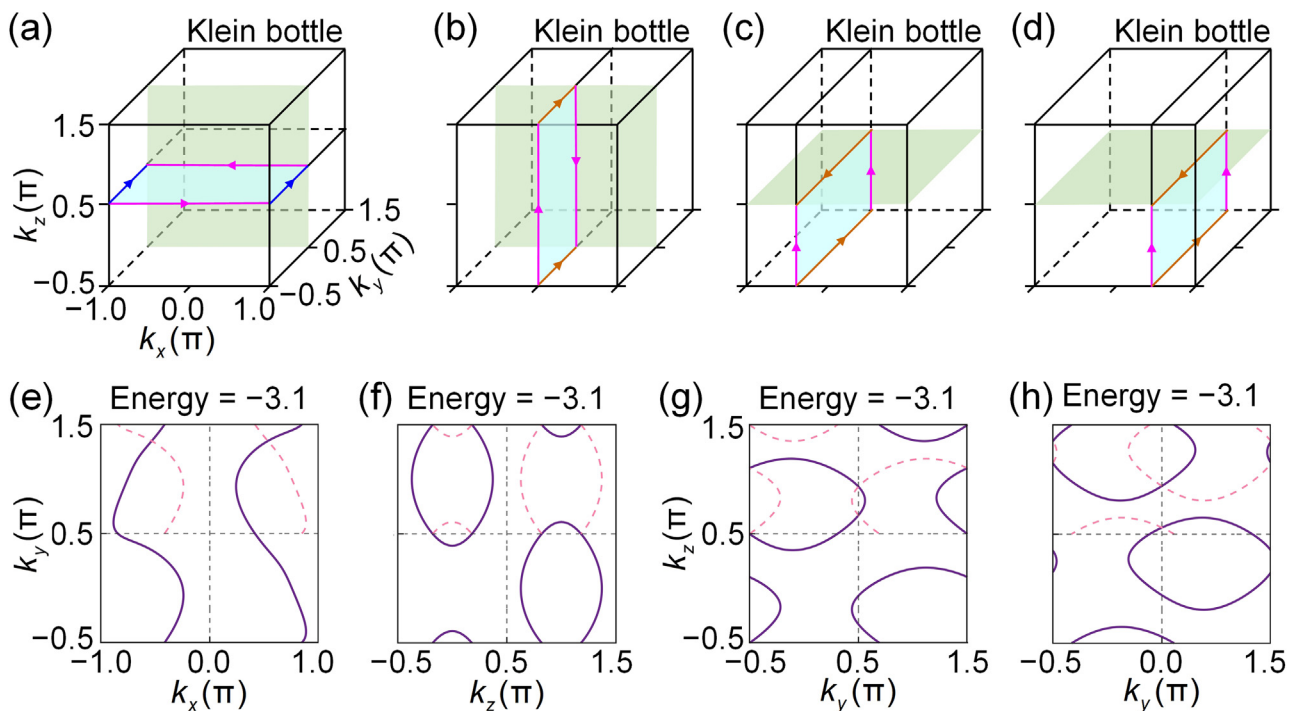


Fig. 2. Brillouin Klein bottles (cyan planes) which are achieved by appropriately cutting the Brillouin half-turn space (a, b) or Klein space (c, d). The marked arrow directions indicate how the boundaries with the same color will be “glued” together. (e–h) The constant energy contours corresponding to the cut 2D BZ in (a–d), respectively. For comparison, the constant energy contours within the lower half 2D BZ are translated to the upper half 2D BZ and marked as pink dashed lines.

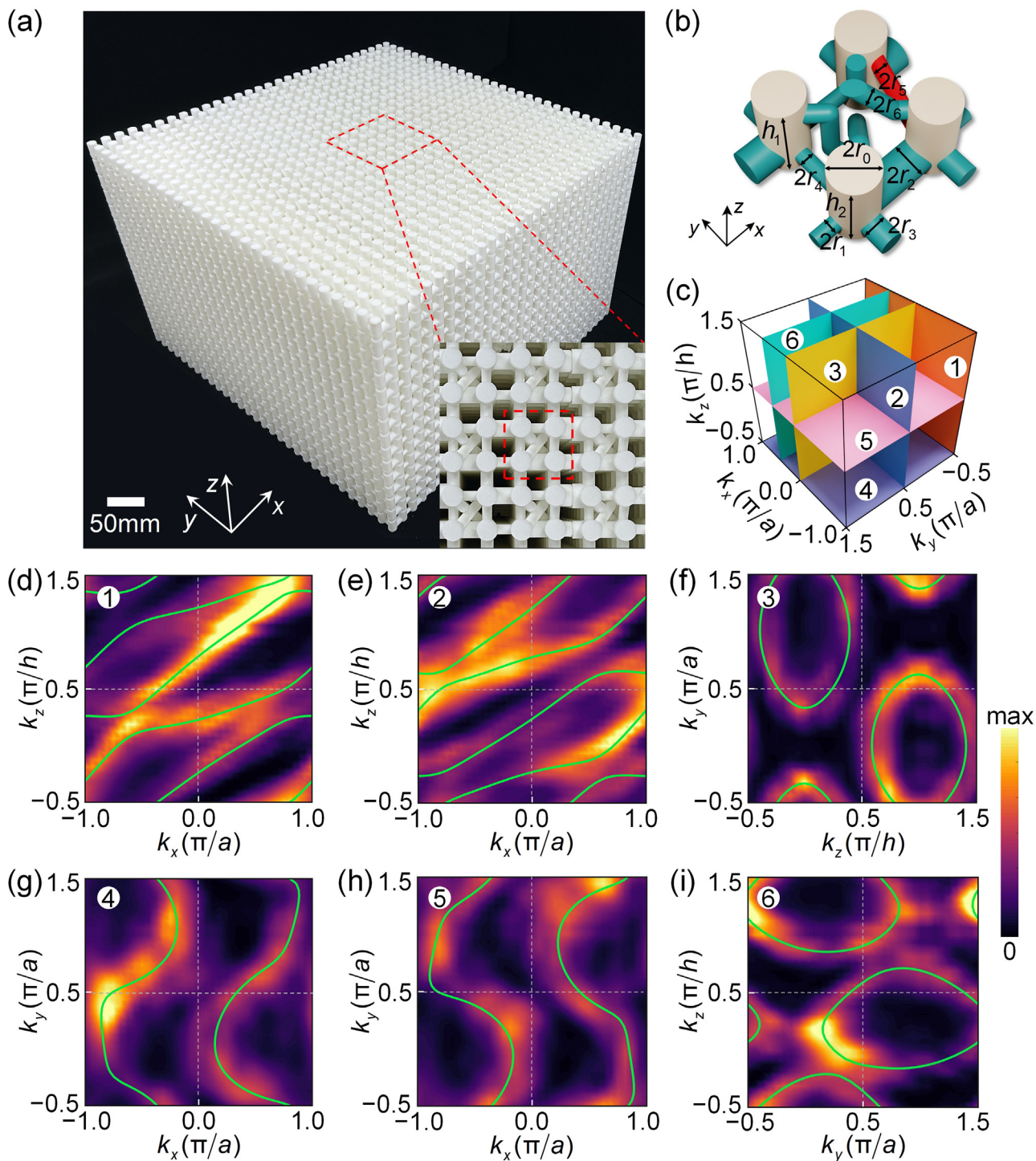


Fig. 3. Observation of Brillouin half-turn space and Klein space. (a) Photograph of the sample. The inset shows a top view of the sample center where the red dashed square denotes a unit cell. (b) A unit cell of the 3D acoustic crystal. The lattice constants in the x - y plane and z -direction are $a = 48$ mm and $h = 32$ mm, and the other geometrical parameters are $r_0 = 6$ mm, $r_1 = 2$ mm, $r_2 = 4.5$ mm, $r_3 = 3$ mm, $r_4 = 2$ mm, $r_5 = 2$ mm, $r_6 = 2.2$ mm, $h_1 = 24.5$ mm, and $h_2 = 24$ mm, respectively. (c) The six colored planes are 2D BZs cut from the 3D Brillouin half-turn space (①–③) or Klein space (④–⑥), respectively. (d–i) Measured (color maps) and simulated (green lines) *iso*-frequency contours of the bulk band structure at 6.46 kHz that correspond to the six cut 2D BZs in (c), respectively.

Next, we demonstrate a non-orientable Brillouin Klein space in the same 3D acoustic crystal. In Fig. 3g, h, after a reflection through the $k_y = 0.5\pi/a$ (horizontal grey dashed line), the measured (color maps) and simulated (green lines) *iso*-frequency contour at fixed $k_z = -0.5\pi/h$ (purple plane in Fig. 3c) in Fig. 3g coincides exactly with that at $k_z = -0.5\pi/h + \pi/h$ (pink plane in Fig. 3c) in Fig. 3h.

Therefore, the half 3D BZ is topologically a non-orientable Brillouin Klein space consisting of layered Brillouin Klein bottles [49] with arbitrarily fixed k_x (see Supplementary materials). Indeed, as shown in Fig. 3i, the measured (color maps) and simulated (green lines) *iso*-frequency contour of the cut 2D BZ with fixed $k_x = 0.5\pi/a$ (cyan plane in Fig. 3c) exhibits similar 2D momentum-space glide

reflection symmetry. Note that a single Brillouin Klein space can also be realized by simply stacking a 2D lattice model with vertical interlayer couplings (see [Supplementary materials](#)).

3.3. Self-collimated topological surface states of stacked weak Klein bottle insulator

Finally, we explore the novel topological surface states of the 3D acoustic crystal. [Fig. 4a](#) shows the calculated topological surface state dispersions on surface 1 (red sheet) and surface 2 (blue sheet), respectively. The frequency-dependent dispersions ([Fig. 4b](#)) along k_y direction with fixed $k_z = 0.5\pi/h$ (vertical grey plane in [Fig. 4a](#)) exhibits a nonlocal twist relation between the two topological surface states. By translating $0.5\pi/a$ along the k_y

direction, the projected surface state dispersion of surface 1 (red line) coincides with that of surface 2 (blue line). This is because the non-symmorphic character of M_x in the 2D momentum space guarantees that only the projected surface state dispersions over $k_y \in [-\pi/2a, \pi/2a]$ are independent, while those over $k_y \in [\pi/2a, 3\pi/2a]$ can be deduced from the operation of M_x . In this case, a topological invariant defined on the cut half 2D BZ (cyan plane in [Fig. 2a](#)) can be given by

$$v = \frac{1}{2\pi} [\gamma(-\pi/2) + \gamma(\pi/2)] \bmod 2, \quad (2)$$

where $\gamma(-\pi/2)$ and $\gamma(\pi/2)$ are the Berry phases on the $k_y = -\pi/2$ and $k_y = \pi/2$ paths, respectively. Considering the specific parameters for our model (see the [Supplementary materials](#)), we obtain a non-

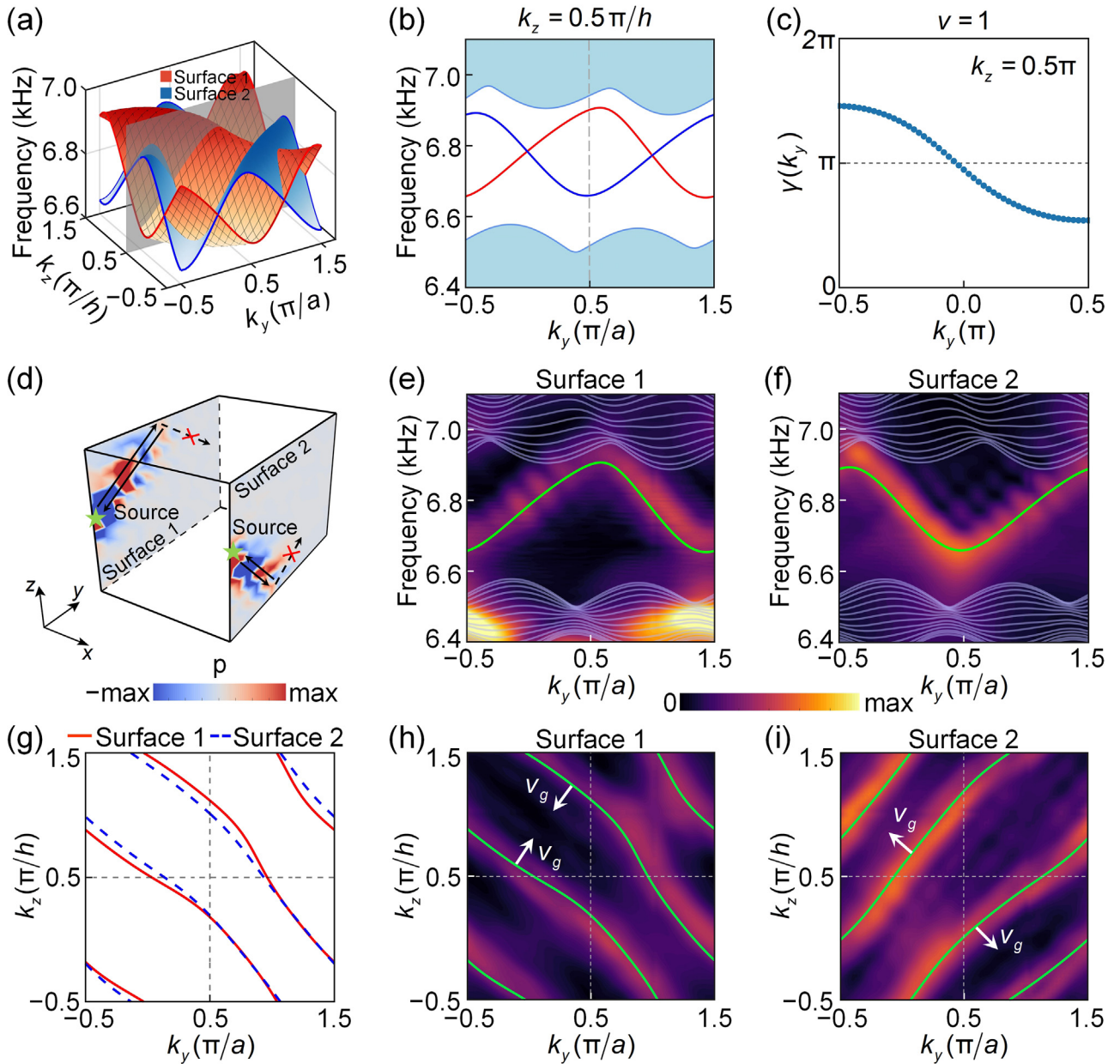


Fig. 4. Stacked weak Klein bottle insulator and its self-collimated topological surface states. (a) Simulated surface dispersions of two surfaces parallel to the y - z plane. (b) Simulated surface dispersions with fixed $k_z = 0.5\pi/h$. (c) The flows of $\gamma(k_y)$ for the cubic lattice model ([Fig. 1a](#)) with fixed $k_z = 0.5\pi$. (d) Measured acoustic field distributions of the self-collimated topological surface states at 6.8 kHz. Green stars are acoustic point sources. (e, f) Measured surface state dispersions with fixed $k_z = 0.5\pi/h$. The white (green) lines indicate the simulated bulk (surface) dispersions. (g) Simulated iso-frequency contour of two surfaces at 6.8 kHz. (h, i) Measured (color maps) and simulated (green lines) iso-frequency contours of surfaces 1 and surface 2, respectively. The white arrows denote group velocity directions of iso-frequency dispersions.

trivial topological invariant $\nu = 1$, as shown in Fig. 4c. This result holds true for all Brillouin Klein bottles cut from the Brillouin half-turn space (see the Supplementary materials). Therefore, similar to the naming of weak topological insulators [50] and weak Stiefel–Whitney insulators [51], we name this 3D acoustic crystal as a stacked weak Klein bottle insulator with nontrivial \mathbb{Z}_2 topological invariant defined over the Brillouin half-turn space that supports novel self-collimated topological surface states (Fig. 4d). The measured topological surface state dispersions (color maps) of two opposite surfaces are shown in Fig. 4e, f, matching well with the simulation results (green lines).

To further explore the peculiar nonlocal twisted relationship between the two surface states, we plot their simulated (Fig. 4g) and measured (Fig. 4h, i) iso-frequency contours. The reflection of the iso-frequency contours of surface 2 (blue dashed lines) through the axis of $k_z = 0.5\pi/h$ (horizontal grey dashed line) almost coincides with that of surface 1 (red solid lines) after a half translation $\mathbf{L}_{G_z/2}$ (Fig. 4g), in which the slight mismatch results from that the tight-binding model is not fully mapped to the realistic acoustic crystal (see the Supplementary materials). Compared with previous 3D acoustic topological insulators [27,52], our acoustic stacked weak Klein bottle insulator exhibits three distinctive properties. Firstly, unlike the divergent topological surface states observed in previous 3D acoustic topological insulators with Dirac conical dispersion relations, our stacked weak Klein bottle insulator features self-collimated topological surface states because of their nearly flat iso-frequency contour, as shown in Fig. 4g. The self-collimated topological surface states hold promise for various acoustic wave manipulations, such as directional vocalization, acoustic beam collimating, and compact waveguiding. Secondly, the self-collimated topological surface states exhibit exotic negative reflection (Fig. 4d) due to the opposite group velocity directions of iso-frequency dispersions (Fig. 4h, i), which can be used as a topological acoustic retroreflector. Thirdly, the iso-frequency contours of the self-collimated topological surface states form an exotic torus link (Hopf link) on the momentum space surface (see the Supplementary materials), in stark contrast to the previously reported torus link formed on the domain wall between two different 3D Chern insulators with perpendicular Chern vectors [15]. Interestingly, gauge symmetry can also be used to realize higher-order Klein bottle insulators with topological hinge states and corner states [53,54].

4. Conclusion and outlook

In conclusion, we have theoretically discovered and experimentally observed a non-orientable Brillouin Klein space and an orientable Brillouin half-turn space in a 3D acoustic crystal with artificial gauge fields. The interplay between artificial gauge fields and symmetry thoroughly changes the algebraic structure of crystalline symmetries, giving rise to peculiar 3D momentum-space non-symmorphic screw rotation and glide reflection symmetries. These features in turn reduce the fundamental domain of 3D momentum space from the usual orientable Brillouin three-torus to a non-orientable Brillouin Klein space or an orientable Brillouin half-turn space, fundamentally modifying the fundamental domain and topology of the 3D BZ. Moreover, we experimentally demonstrate a novel stacked weak Klein bottle insulator with self-collimated topological surface states. Our work provides a powerful platform to explore the theory of momentum-space non-symmorphic symmetry [55] and the novel multidimensional manifold topologies of momentum space as well as the gauge-symmetry-enriched topological physics that are beyond the scope of topological materials. We envision that other novel momentum-space multidimensional manifold topologies, such as quarter-turn

space [49], hexagonal torus [49], and Roman surface [56] can also be realized in acoustic crystals with artificial gauge fields.

Conflict of interest

The authors declare that they have no conflict of interest.

Acknowledgments

Zhen Gao acknowledges funding from the National Natural Science Foundation of China (62375118, 6231101016, and 12104211), Shenzhen Science and Technology Innovation Commission (20220815111105001), and SUSTech (Y01236148 and Y01236248). Zhengyou Liu acknowledges funding from the National Key R&D Program of China (2022YFA1404900 and 2018YFA0305800), and the National Natural Science Foundation of China (11890701). Yan Meng acknowledges the support from the National Natural Science Foundation of China (12304484), Basic and Applied Basic Research Foundation of Guangdong Province (2414050002552), and Shenzhen Science and Technology Innovation Commission (202308073000209). Perry Ping Shum acknowledges the National Natural Science Foundation of China (62220106006), and Shenzhen Science and Technology Program (SGDX20211123114001001). Kexin Xiang acknowledges the Special Funds for the Cultivation of Guangdong College Students' Scientific and Technological Innovation (pdjh2023c21002).

Author contributions

Zhen Gao initiated the project. Zhenxiao Zhu, Gui-Geng Liu, Linyun Yang, and Yan Meng performed the theoretical calculation. Zhenxiao Zhu, Xiang Xi, and Bei Yan performed the simulation. Zhenxiao Zhu, Zhen Gao, Gui-Geng Liu, and Zhengyou Liu designed the experiments. Zhenxiao Zhu, Jien Wu, Weiyin Deng, Xueqin Huang, and Jiuyang Lu carried out the measurements. Zhenxiao Zhu, Linyun Yang, Yan Meng, Xiang Xi, Bei Yan, Jingming Chen, Ce Shang, Perry Ping Shum, Hongsheng Chen, Yihao Yang, Kexin Xiang, Gui-Geng Liu, and Zhen Gao analyzed the results. Zhenxiao Zhu and Zhen Gao wrote the manuscript with input from all authors. Zhen Gao, Gui-Geng Liu and Zhengyou Liu supervised the project.

Appendix A. Supplementary materials

Supplementary materials to this article can be found online at <https://doi.org/10.1016/j.scib.2024.05.003>.

References

- [1] Bloch F. Über die Quantenmechanik der Elektronen in Kristallgittern. *Z Phys* 1929;52:555–600.
- [2] Brillouin L. Les électrons libres dans les métaux et le rôle des réflexions de Bragg. *J Phys Radium* 1930;1:377–400.
- [3] Giustino F. Electron-phonon interactions from first principles. *Rev Mod Phys* 2019;91:019901.
- [4] Bansil A, Lin H, Das T. Colloquium: Topological band theory. *Rev Mod Phys* 2016;88:021004.
- [5] Ma S, Yang B, Zhang S. Topological photonics in metamaterials. *Photon Insights* 2022;1:R02.
- [6] Ni X, Yves S, Krasnok A, et al. Topological metamaterials. *Chem Rev* 2023;123:7585–654.
- [7] Yablonovitch E. Inhibited spontaneous emission in solid-state physics and electronics. *Phys Rev Lett* 1987;58:2059–62.
- [8] John S. Strong localization of photons in certain disordered dielectric superlattices. *Phys Rev Lett* 1987;58:2486–9.
- [9] Haldane FDM. Model for a quantum Hall effect without Landau levels: Condensed-matter realization of the “parity anomaly”. *Phys Rev Lett* 1988;61:2015–8.

- [10] Wang Z, Chong Y, Joannopoulos JD, et al. Observation of unidirectional backscattering-immune topological electromagnetic states. *Nature* 2009;461:772–5.
- [11] Lu L, Joannopoulos JD, Soljačić M. Topological photonics. *Nat Photon* 2014;8:821–9.
- [12] Ozawa T, Price HM, Amo A, et al. Topological photonics. *Rev Mod Phys* 2019;91:015006.
- [13] Xie L, Jin L, Song Z. Antihelical edge states in two-dimensional photonic topological metals. *Sci Bull* 2023;68:255–8.
- [14] Yang Y, Gao Z, Xue H. Realization of a three-dimensional photonic topological insulator. *Nature* 2019;565:622–6.
- [15] Liu GG, Gao Z, Wang Q, et al. Topological Chern vectors in three-dimensional photonic crystals. *Nature* 2022;609:925–30.
- [16] Kushwaha M, Halevi P, Dobrzynski L, et al. Acoustic band structure of periodic elastic composites. *Phys Rev Lett* 1993;71:2022–5.
- [17] Yang Z, Gao F, Shi X, et al. Topological acoustics. *Phys Rev Lett* 2015;114:114301.
- [18] Khanikaev AB, Fleury R, Mousavi SH, et al. Topologically robust sound propagation in an angular-momentum-biased graphene-like resonator lattice. *Nat Commun* 2015;6:8260.
- [19] He C, Ni X, Ge H, et al. Acoustic topological insulator and robust one-way sound transport. *Nat Phys* 2016;12:1124–9.
- [20] Ding Y, Peng Y, Zhu Y, et al. Experimental demonstration of acoustic Chern insulators. *Phys Rev Lett* 2019;122:014302.
- [21] Wu Y, Yan M, Lin ZK, et al. On-chip higher-order topological micromechanical metamaterials. *Sci Bull* 2021;66:1959–66.
- [22] Hu B, Zhang Z, Zhang H, et al. Non-Hermitian topological whispering gallery. *Nature* 2021;597:655–9.
- [23] Huang X, Lu J, Yan Z, et al. Acoustic higher-order topology derived from first-order with built-in Zeeman-like fields. *Sci Bull* 2022;67:488–94.
- [24] Liao D, Liu Y, Zhang Z, et al. Synthesizing topological acoustic rainbow trapping at deep-subwavelength corners. *Sci Bull* 2023;68:1744–2177.
- [25] Wu SQ, Cheng W, Liu XY, et al. Observation of D-class topology in an acoustic metamaterial. *Sci Bull* 2024;69:893–900.
- [26] He H, Qiu C, Ye L, et al. Topological negative refraction of surface acoustic waves in a Weyl acoustic crystal. *Nature* 2018;560:61–4.
- [27] He C, Lai HS, He B, et al. Acoustic analogues of three-dimensional topological insulators. *Nat Commun* 2020;11:2318.
- [28] Lin Z, Wu Y, Jiang B, et al. Topological Wannier cycles induced by sub-unit-cell artificial gauge flux in a sonic crystal. *Nat Mater* 2022;21:430–7.
- [29] Xue H, Yang Y, Zhang B. Topological acoustics. *Nat Rev Mater* 2022;7:974–90.
- [30] Xu C, Zheng T, Hao Ge, et al. Topological boundary states transport in synthetic four-dimensional acoustic system. *Sci Bull* 2022;67:1950–3.
- [31] Ningyuan J, Owens C, Sommer A, et al. Time- and site-resolved dynamics in a topological circuit. *Phys Rev X* 2015;5:021031.
- [32] Imhof S, Berger C, Bayer F, et al. Topoelectrical-circuit realization of topological corner modes. *Nat Phys* 2018;14:925–9.
- [33] Wang P, Lu L, Bertoldi K. Topological phononic crystals with one-way elastic edge waves. *Phys Rev Lett* 2015;115:104302.
- [34] Huber SD. Topological mechanics. *Nat Phys* 2016;12:621–3.
- [35] Ma G, Xiao M, Chan CT. Topological phases in acoustic and mechanical systems. *Nat Rev Phys* 2019;1:281–94.
- [36] Cooper NR, Dalibard J, Spielman IB. Topological bands for ultracold atoms. *Rev Mod Phys* 2019;91:015005.
- [37] Shao L, Liu Q, Xiao R, et al. Gauge-field extended $k \cdot p$ method and novel topological phases. *Phys Rev Lett* 2021;127:076401.
- [38] Zhao Y, Huang Y, Yang SA. Z_2 -projective translational symmetry protected topological phases. *Phys Rev B* 2020;102:161117(R).
- [39] Xue H, Wang Z, Huang Y, et al. Projectively enriched symmetry and topology in acoustic crystals. *Phys Rev Lett* 2022;128:116802.
- [40] Li T, Du J, Zhang Q, et al. Acoustic Möbius insulators from projective symmetry. *Phys Rev Lett* 2022;128:116803.
- [41] Li T, Liu L, Zhang Q, et al. Acoustic realization of projective mirror Chern insulators. *Commun Phys* 2023;6:268.
- [42] Shao L, Chen Z, Wang K, et al. Spinless mirror Chern insulator from projective symmetry algebra. *Phys Rev B* 2023;108:205126.
- [43] Zhao Y, Chen C, Sheng XL, et al. Switching spinless and spinful topological phases with projective PT symmetry. *Phys Rev Lett* 2021;126:196402.
- [44] Meng Y, Lin S, Shi B, et al. Spinful topological phases in acoustic crystals with projective PT symmetry. *Phys Rev Lett* 2023;130:206101.
- [45] Chen Z, Zhang Z, Yang SA, et al. Classification of time-reversal-invariant crystals with gauge structures. *Nat Commun* 2023;14:743.
- [46] Xue H, Chen Z, Cheng Z, et al. Stiefel-Whitney topological charges in a three-dimensional acoustic nodal-line crystal. *Nat Commun* 2023;14:4563.
- [47] Xiang X, Ni X, Gao F et al. Demonstration of acoustic high-order Stiefel-Whitney semimetal in bilayer graphene sonic crystals. arXiv:2304.12735, 2023.
- [48] Chen Z, Yang SA, Zhao Y. Brillouin Klein bottle from artificial gauge fields. *Nat Commun* 2022;13:2215.
- [49] Weeks JR. *The Shape of Space*. Boca Raton: CRC Press; 2020.
- [50] Fu L, Kane CL, Mele EJ. Topological insulators in three dimensions. *Phys Rev Lett* 2007;98:106803.
- [51] Ahn J, Park S, Kim D, et al. Stiefel-Whitney classes and topological phases in band theory. *Chin Phys B* 2019;28:117101.
- [52] Yang L, Wang Y, Meng Y, et al. Observation of Dirac hierarchy in three-dimensional acoustic topological insulators. *Phys Rev Lett* 2022;129:125502.
- [53] Li CA, Sun J, Zhang SB, et al. Klein-bottle quadrupole insulators and Dirac semimetals. *Phys Rev B* 2023;108:235412.
- [54] Tao YL, Yan M, Peng M, et al. Higher-order Klein bottle topological insulator in three-dimensional acoustic crystals. *Phys Rev B* 2024;109:134107.
- [55] Zhang C, Chen Z, Zhang Z, et al. General theory of momentum-space nonsymmorphic symmetry. *Phys Rev Lett* 2023;130:256601.
- [56] Liu G, Pi M, Zhou L, et al. Physical realization of topological Roman surface by spin-induced ferroelectric polarization in cubic lattice. *Nat Commun* 2022;13:2373.



Zhenxiao Zhu received his Ph.D. degree in Physical Electronics from South China University of Technology in 2021. He was a postdoctoral fellow, and is currently serving as a research scientist at Southern University of Science and Technology. His research interest includes topological acoustics and photonics.



Linyun Yang received his B.S. and Ph.D. degrees in Mechanics from Harbin Institute of Technology in 2016 and 2021, respectively. He was a visiting scholar at the Paris Institute of Nanosciences, Sorbonne University from 2019 to 2021. He was a postdoctoral fellow, and is currently serving as a research scientist at Southern University of Science and Technology. His research interest includes topological elastic metamaterials, acoustic and photonic crystals.



Jien Wu received his Ph.D. degree in Physics from South China University of Technology in 2021. He is currently a postdoctoral fellow at South China University of Technology. His research interest includes Hermitian and non-Hermitian topological properties in phononic crystals and electric circuits.



Gui-Geng Liu received his B.S. degree from Nankai University in 2017, and Ph.D. degree from Nanyang Technological University in 2023. He is currently a Research Fellow at Nanyang Technological University and a future assistant professor at Westlake University. His research interest includes topological photonics and non-Hermitian physics.



Zhengyou Liu received his Ph.D. degree in 1993 from Wuhan University. Before he joined Wuhan University in 2001, he held the position of a professor at South China University of Technology. He is currently a professor at the School of Physics and Technology. His current research interest includes wave physics, phononic crystals and acoustic metamaterials, acoustic radiation force and particle manipulation, and topological acoustics.



Zhen Gao received his Ph.D. degree in Applied Physics from Nanyang Technological University in 2018. In 2021, he joined Southern University of Science and Technology as an associate professor. His research interest includes topological photonics/acoustics/electric circuits, photonic crystals, metamaterials and integrated photonics.